SCIENCE CHINA Materials

LETTERS

mater.scichina.com link.springer.com

Published online 14 November 2018 | https://doi.org/10.1007/s40843-018-9366-x

Sci China Mater 2019, 62(2): 273–282

Ultrathin yet transferrable Pt- or PtRu-decorated graphene films as efficient electrocatalyst for methanol oxidation reaction

Zhuchen Tao[1†], Wei Chen[2†], Jing Yang[2], Xiangyang Wang[1], Ziqi Tan[1], Jianglin Ye[1], Yanxia Chen[2*] and Yanwu Zhu[1*]

Direct methanol fuel cell (DMFC) has been regarded as one of promising electric generators in portable electronic equipment and electric vehicles because of the high energy conversion efficiency and low pollutant emissions [1,2]. Electro-oxidation of methanol has been studied extensively in terms of its application in DMFC and related theoretical analysis [3–5]. To date, the most promising anode catalyst for methanol oxidation is platinum (Pt). However, the development of commercial Pt-based fuel cells has been limited by the toxicity of carbon monoxide, the high cost of Pt and the aggregation of catalyst particles [6–9]. Using binary or alloy catalysts is an effective strategy for the removal of CO from the catalyst surface [10–13]. Extensive research reveals that ruthenium (Ru)-modified Pt nanoparticles (Pt NPs) are efficient binary electro-catalysts for methanol oxidation reaction (MOR) [14]. The addition of Ru to Pt-based catalysts significantly lowers the overpotential in MOR and enhances the CO-tolerance through the 'bifunctional mechanism' [11,12,14–18].

Considerable efforts have been devoted to reducing the amount of Pt by using various Pt-carbon hybrids, such as Pt-carbon nanotubes (Pt-CNTs) [19], Pt-porous carbons [20], and Pt-graphene [21]. Graphene is such a substrate that has a large specific surface area (for high catalyst loading), good stability (for tolerance to harsh conditions) as well as a high electrical conductivity (for efficient electron transfer) and therefore has been considered as a promising catalyst carrier in DMFCs [22,23]. With oxygen-containing functional groups, graphene oxide (GO) is able to promote the growth of the metal NPs [24], and thus hybridizing graphene materials derived from GO with catalytic metals has been developed [25,26]. Particularly, Pt-decorated three-dimensional (3D) graphene hybrids exhibit improved electro-catalytic performances owing to the excellent dispersion of Pt NPs in the porous carbon architectures [27–32]. However, the large amount of defects and impurity in the graphene derived from GO substantially hinders the electrical and mechanical properties of the hybrid catalysts [33,34]. The defects may cause the graphene-based hybrids significantly unstable under harsh electrochemical conditions because of higher activity at the sites of defects [35]; the re-stacking and agglomeration in GO-based materials also impede the functionalization of graphene in the hybrids. The good stability and excellent conductivity of graphene from chemical vapor deposition (CVD) bring a high-quality and neat platform to evaluate the role of carbon in catalytic hybrids [36], but the surface of graphene produced by CVD (CVDG) is inactive due to its high degree of graphitization and thus it is challenging to directly deposit highly dispersed metal NPs [37]. Till now, CVDG has not been used to carry metal NPs for catalysis.

Herein, we demonstrate that controlled dispersion of Pt NPs with special particle size is realized on gently-modified CVDG using a mild and environmentally friendly reductant, ethylene glycol (EG), in a hydrothermal process. The obtained ultrathin Pt NPs/CVDG (Pt-CVDG) hybrid films are different from the previously reported hybrids in which pre-synthesized metal NPs

[1] CAS Key Laboratory of Materials for Energy Conversion; Department of Materials Science and Engineering; i-ChEM, University of Science and Technology of China, Hefei 230026, China

[2] Hefei National Laboratory for Physical Sciences at Microscale, Department of Chemical Physics; University of Science and Technology of China, Hefei 230026, China

† These authors contributed equally to this paper.

* Corresponding authors (emails: yachen@ustc.edu.cn (Chen Y); zhuyanwu@ustc.edu.cn (Zhu Y))

were hybridized with graphene substrates by covalent bonding [38], electrostatics [39] or ligand-metal ion-ligand bridges [40], as these kinds of connections often lead to dramatic decrease in catalytic activity. The Pt-CVDG films can be transferred to other substrates due to high mechanical strength of CVDG, using common method performed on intrinsic CVDG [41]. Due to the monolayer feature of CVDG, the mass loading of Pt in Pt-CVDG hybrids is above 80 wt.%, much higher than that of traditional Pt-carbon hybrid catalyst (20 wt.%) [28–31,42–48]. The evaluation of Pt-CVDG catalysts for MOR shows a low onset potential at 0.40 V *vs.* Ag/AgCl, and a high mass specific current density of 293.1 mA mg^{-1}_{Pt} in forward scan, with a forward/reverse scan peak current ratio of 1.33 for a Pt loading of 3.15 μg cm^{-2} measured in the voltage range of 0–1.0 V. When Ru is electrochemically deposited onto the surface of Pt-CVDG film (with a Pt loading of 5.49 μg cm^{-2}), the onset potential of the PtRu-CVDG film electrode (for a nominal Pt and Ru coverage ratio of 68:32) is 0.20 V-more negative than that for Pt-CVDG film, and its mass activity (280.3 mA mg^{-1}_{Pt} at 0.5 V *vs.* Ag/AgCl) is about 2.5 times better than the latter measured in the voltage range of −0.20 to 0.50 V.

As shown in Fig. 1, monolayer graphene was synthesized on copper foils by a low pressure CVD [49], and then transferred onto SiO_2/Si substrates [41]. Oxygen plasma treatment was carried out to create oxygen-containing functional groups, resulting in negative charges on the surface of the graphene [50]. Raman spectrum (Fig. S1b) of CVDG transferred on Si/SiO_2 confirms the features of uniform monolayer graphene with intensity ratio (~2.0) of 2D (2,682 cm^{-1}) to G (1,584 cm^{-1}) band and the full width at half maximum (FWHM) (33.1 cm^{-1}) of the 2D band. The absence of D (1,350 cm^{-1}) band indicates the high quality of the CVDG prepared [51]. After being exposed to a mildly O_2 plasma, the Raman spectrum in Fig. S1b shows the appearance of D band which is relevant to defects in graphitic materials, especially when compared to the G band [51]. However, the decrease in the I_D/I_G ratio after the hydrothermal process (Fig. S1d) indicates that the gentle O_2 plasma has mostly introduced oxygen-containing groups noncovalently-bonded in close proximity to the carbon atoms arranged in benzene rings [52]. After treatment with oxygen plasma from 1 to 8 s, the sheet resistance is increased by about 1 to 3 times, which is still 1 to 2 order of magnitude higher than those from reduced graphene oxide (RGO), as shown in Fig. S1f and previous reports [53]. A gradual attenuation as well as a slight broadening of 2D band is observed with increase the exposure time from 1 to 8 s with a plasma power of 10 W. But the FWHM of 2D peak recovers to the original value after hydrothermal process (Fig. S1e), further proving that the plasma treatment does not induce significant structural

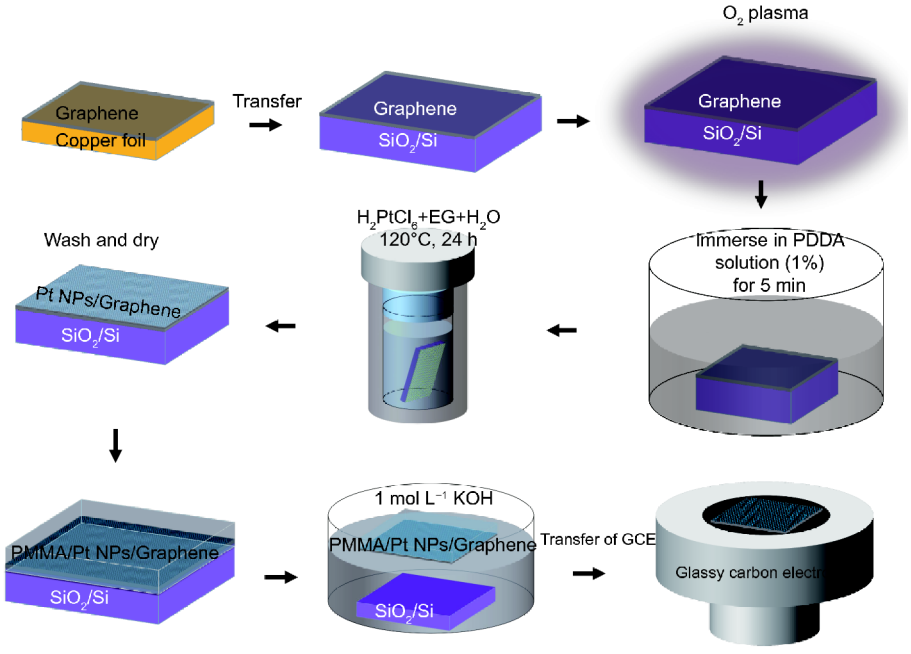

Figure 1 Schematic illustration of the synthesis of Pt-CVDG films. The procedure includes transfer of graphene films on desired substrates (SiO_2/Si

defects in graphene. After the O_2 plasma treatment, a cationic polyelectrolyte, poly(dimethyldiallylammonium chloride) (PDDA), was applied on the negatively charged CVDG, resulting in a positively-charged surface [54]. After the sequential washing and drying, the sample was sealed in a 50-mL autoclave equipped with 30 mL of chloroplatinic acid (H_2PtCl_6) solution in ethylene glycol-water (5:1) and kept at 180°C for 24 h, for the deposition of Pt NPs [27,55]. Then the sample was taken out and washed several times with ethanol to remove residual chloride ions. The SEM images in Figs S2 and S3 show that the coverage of Pt NPs on CVDG is sensitive to the duration of O_2 plasma treatment and that of PDDA treatment. The O_2 plasma treatment for 4 s with a power of 10 W and a PDDA solution treatment for 5 min were typically used to obtain the samples with uniform coverage of Pt NPs on CVDG and minimizing the structural defects. Finally, the resulting sample was dried and transferred to a glassy carbon electrode (GCE) by a poly(methyl methacrylate) (PMMA) assisted method for electrochemical evaluation.

The as-prepared Pt-CVDG films were examined with scanning electron microscopy (SEM) and transmission electron microscopy (TEM). The mass density of Pt NPs can be adjusted by the concentration of H_2PtCl_6 in the hydrothermal process mentioned above; Pt-CVDG films with Pt loading of 6.24, 5.49 and 3.15 μg cm^{-2} as determined by inductively coupled plasma mass spectrometer (ICP-MS), are denoted as Pt-CVDG-1, Pt-CVDG-2, and Pt-CVDG-3, respectively. Based on the density of monolayer graphene (0.77 mg m^{-2}), the Pt loading on Pt-CVDG films can be estimated as 89.0, 87.6 or 80.3 wt.% for Pt-CVDG-1, Pt-CVDG-2 or Pt-CVDG-3, respectively. As shown in the SEM images in Fig. 2a–c, all samples have a uniform coverage of particles. The corresponding HRTEM images (Fig. 2g–i) clearly show the lattice fringes of Pt NPs, in which the typical interlayer distances of 0.223 nm and 0.195 nm are attributed to the interlayer spacings of (111) and (100) planes in face-centered cubic (fcc) Pt structure [56]. The Pt NPs aggregated on the graphene surface and had diameters of 2–5 nm. The size-distribution histograms (Fig. 2j–i) of the Pt NPs, obtained by measuring about 100 randomly-selected particles for each HRTEM image, show the average size of about 3.34, 3.29 and 3.25 nm, for Pt-CVDG-1, Pt-CVDG-2 and Pt-CVDG-3, respectively. Although the monolayer graphene is invisible from the SEM and HRTEM images, the selected area electron diffraction (SAED) pattern (in Fig. 2m) taken on Pt-CVDG-2 shows the weak yet visible six-fold symmetry diffraction of monolayer graphene [57,58], in addition to the multiple diffraction rings which are ascribed to Pt crystalline reflections of (111), (200), (220) and (311). Furthermore, X-ray photoelectron spectroscopy (XPS) was carried out to analyze the electronic structure of the Pt-CVDG and the typical XPS spectra of Pt-CVG-2 are shown in Fig. S4a, b. The C 1s spectrum of Pt-CVDG-2 in Fig. S4a has been fitted with four peaks. The most intense one at the binding energy of 284.7 eV corresponds to C–C bonding, and the other three peaks at 286.4, 287.9 and 288.9 eV are ascribed to C–O, C=O and O–C=O, respectively, indicating the existence of oxygen containing functional groups in CVDG after O_2 plasma treatment [27]. The Pt 4f spectrum shown in Fig. S4b consists of three pairs of doublets. The most intensive one at 71.5 and 74.75 eV is contributed to Pt^0 $4f_{7/2}$ and Pt^0 $4f_{5/2}$, while the other two weak doublets at 72.6/75.7 and 75.3/76.75 eV correspond to Pt^{2+} and Pt^{4+}, respectively. The metallic Pt^0 contributes to 75.2% in the whole Pt content [59].

The electrochemical behavior of Pt-CVDG films was investigated by means of cyclic voltammograms (CVs) [27]. Fig. 3a shows the representative CV curves of Pt-CVDG/GCE and Pt/C/GCE in 1.0 mol L^{-1} H_2SO_4. Electrochemically active surface area (ECSA) of all the above catalysts were estimated by calculating the coulombic charge for hydrogen adsorption and assuming that the oxidation of full monolayer of H atoms on polycrystalline Pt corresponds to a charge density of 210 μC cm^{-2} (Table 1). We can see that the very little electric double layer capacitance provided by CVDG compared to Pt-CVDG from Fig. S5 [36]. The results in Table 1 show that all the Pt-CVDG films have higher ECSA values than Pt/C and the highest ECSA is obtained from Pt-CVDG-3 (94.1 m^2 g^{-1}) which is about 3 times higher than that from Pt/C catalyst (28.5 m^2 g^{-1}, 14.15 μg cm^{-2}) under the same conditions, suggesting that the Pt-CVDG possesses a higher dispersion and utilization of Pt NPs. The peak near 0.0 V in Fig. 3a indicates the adsorption of hydrogen on the Pt fcc (100) surface site (I), and that near −0.10 V is ascribed to the adsorption of hydrogen on the fcc (111) stage site (II) (Fig. 3a) [60]. It has been suggested that fcc (100) surface has better electro-catalytic activity than fcc (111) surface for MOR due to its higher oxygen species adsorption capacity [61]. The ratio of the peak current (I) to (II) adsorption of hydrogen are 0.80, 0.81 and 0.79 for Pt-CVDG-1, Pt-CVDG-2 and Pt-CVDG-3, which is much higher than 0.58 in Pt/C, indicating that the Pt-CVDG films are more MOR-active than Pt/C. The MOR performance was investigated by CVs in the mixture of

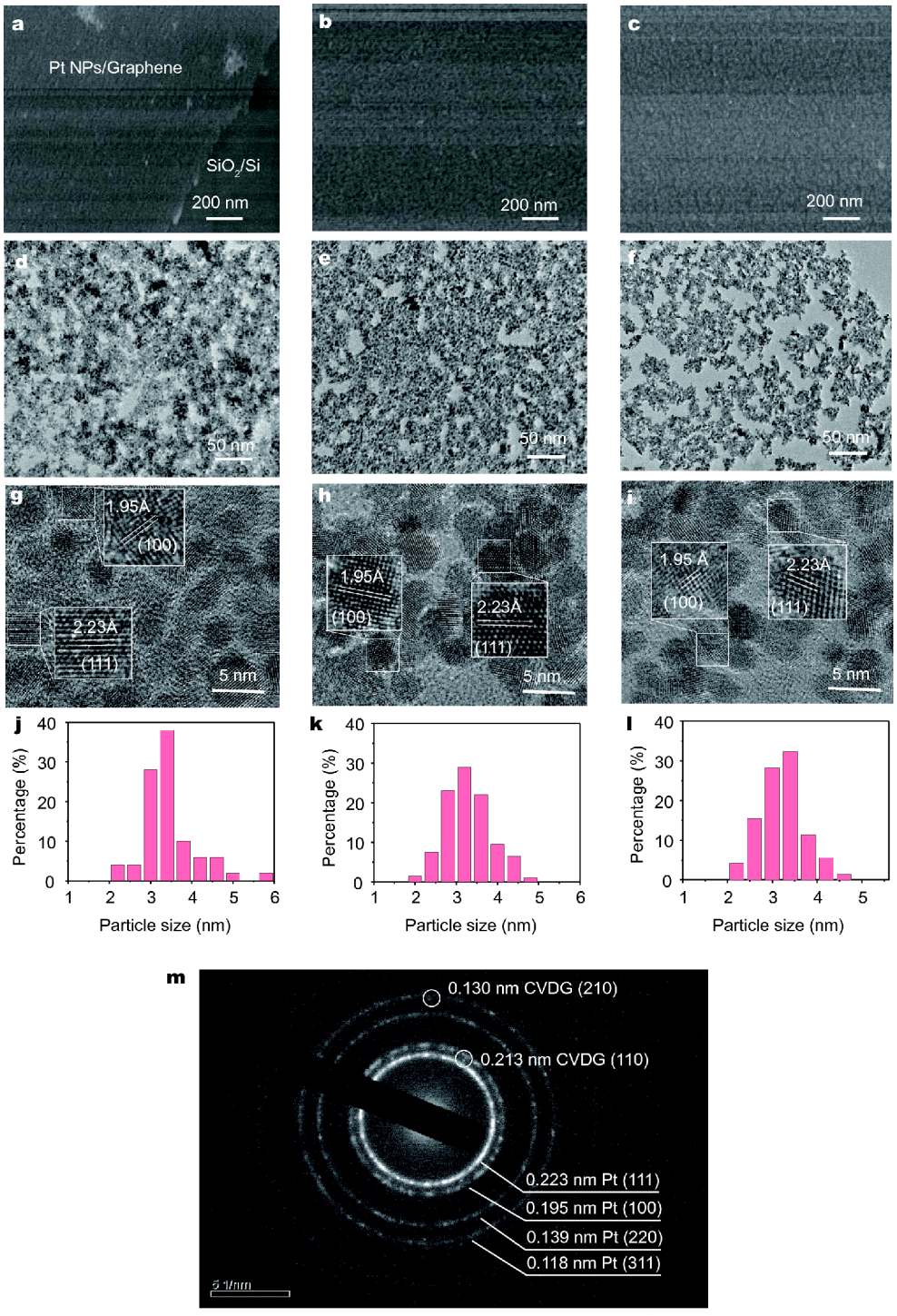

Figure 2 SEM images of Pt-CVDG films for (a) Pt-CVDG-1 (b) Pt-CVDG-2, and (c) Pt-CVDG-3. TEM images of Pt-CVDG films suspended on lacey support film corresponding to (d) Pt-CVDG-1, (e) Pt-CVDG-2 and (f) Pt-CVDG-3, respectively. HRTEM images of (g) Pt-CVDG-1, (h) Pt-CVDG-2, (i) Pt-CVDG-3, with insets showing the corresponding lattice fringes of the NPs marked in the dashed squares, respectively. Size distribution of Pt NPs from (j) Pt-CVDG-1, (k) Pt-CVDG-2 and (l) Pt-CVDG-3. (m) Typical SAED pattern taken from Pt-CVDG-2.

Table 1 Catalytic performance of Pt-CVDG films with different loadings of Pt. ECSA and I_F, I_R, I_F/I_R of Pt-CVDG films were investigated by means of CVs in 1.0 mol L^{-1} H_2SO_4 solution and 1.0 mol L^{-1} H_2SO_4 + 2.0 mol L^{-1} CH_3OH solution, respectively.

Electrode	Loading amount of Pt (mg cm^{-2})	ECSA (m^2 g^{-1})	I_F (mA mg^{-1}_{Pt})	I_R (mA mg^{-1}_{Pt})	I_F/I_R
Pt-CVDG-1	6.24	68.1	225.5	193.5	1.17
Pt-CVDG-2	5.49	60.3	237.4	179.4	1.32
Pt-CVDG-3	3.15	94.1	293.1	235.3	1.24
Pt/C	14.15	28.5	134	193.8	0.72

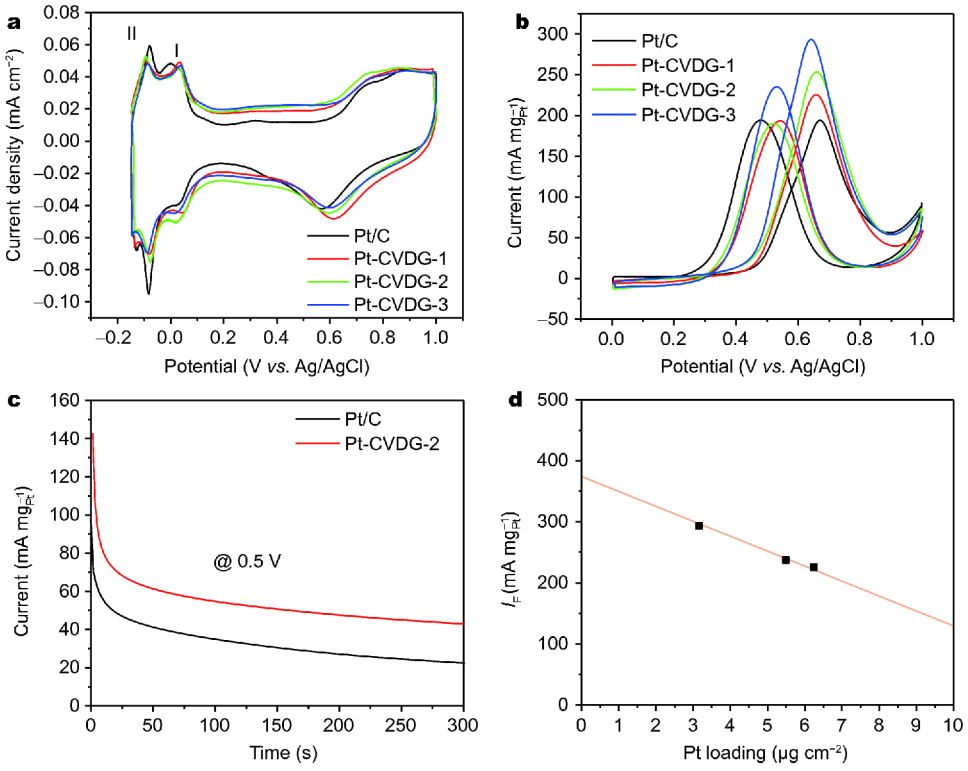

Figure 3 CVs of Pt-CVDG films recorded in (a) 1.0 mol L^{-1} H_2SO_4 solution at a scan rate of 20 mV s^{-1}, and (b) in 1.0 mol L^{-1} H_2SO_4 + 2.0 mol L^{-1} CH_3OH solution at a scan rate of 20 mV s^{-1}. (c) Current evolution for MOR on Pt/C and Pt-CVDG-2/GC electrodes at 0.50 V. (d) Dependence of anodic peak current density in the forward scan on the Pt mass loading. The red line indicates a linear fitting of the data.

1.0 mol L^{-1} H_2SO_4 + 2.0 mol L^{-1} CH_3OH solution (Fig. 3b). The specific current at the peak potential in the forward scan follows the order of Pt-CVDG-3 (293.1 mA mg^{-1}_{Pt}) > Pt-CVDG-2 (253.4 mA mg^{-1}_{Pt}) > Pt-CVDG-1 (225.5 mA mg^{-1}_{Pt}). The specific current at the peak potential decreases with the increase of Pt loading, due to the agglomeration of NPs. And a slight increase of the onset potential for MOR (forward scan) is observed when comparing Pt-CVDG with Pt/C. It is worth noting that Pt-CVDG has a Pt mass loading of more than 80 wt.%, while the Pt loading in Pt/C is 20 wt.%. To investigate the long-term stability, chronoamperometric measurements of Pt-CVDG-2 and Pt/C were performed at 0.50 V for 300 s. As shown in Fig. 3c, Pt-CVDG-2 retains the higher oxidation current over the testing time, displaying the better electro-catalytic durability than Pt/C catalysts for MOR. On the other hand, we also calculated the ratio of forward-scan peak current (I_F) *versus* reverse-scan peak current (I_R), I_F/I_R, which is a key index for evaluating the catalyst tolerance to the accumulation of intermediate carbonaceous species. The ratio for Pt-CVDG-1, Pt-CVDG-2, Pt-CVDG-3 and commercial Pt/C is calculated as 1.17, 1.33, 1.24 and 0.72, respectively. Thus Pt-CVDG films

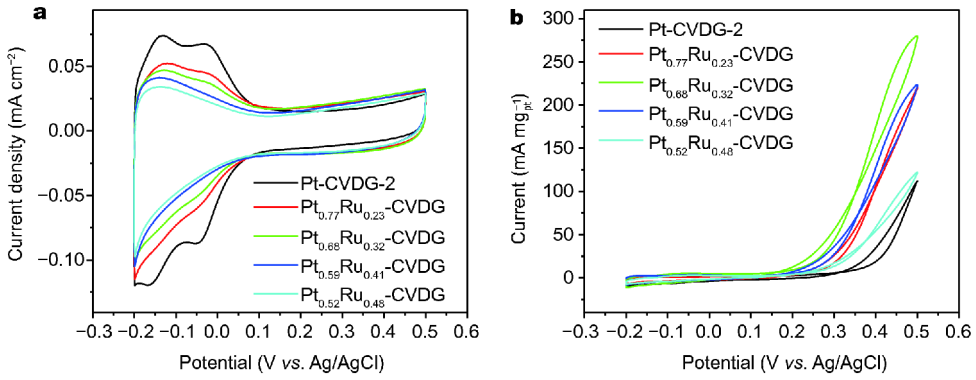

Figure 4 CVs of Pt-CVDG-2 and PtRu-CVDG with different Pt/Ru ratios recorded in (a) 0.1 mol L^{-1} $HClO_4$ solution at a scan rate of 50 mV s^{-1}, and (b) 0.1 mol L^{-1} $HClO_4$ + 2.0 mol L^{-1} CH_3OH solution at a scan rate of 20 mV s^{-1}.

generally have less carbonaceous accumulation and hence are much more tolerant toward CO [27,62]. Both the mass activity and the anti-poisoning ability of Pt-CVDG films are superior to most of Pt-based nanostructures with Pt NPs about 3 nm in diameter (Table S1, Supporting information) [28–31,42,43,45–47]. All the results above indicate that with ultrahigh ECSA and a record-high mass activity for MOR, Pt-CVDG films possess much higher catalytic efficiency and utilization than commercial Pt/C.

Such high utilization of Pt atoms may be due to the uniform distribution and sub-monolayer coverage of Pt NPs on the CVDG, and the preferential fcc (100) orientation of Pt NPs is another reason for their high MOR activity. Based on the above data, we prepared samples of three different Pt loadings. The mass specific I_F increases with the decrease of loading, due to the agglomeration of Pt NPs. From the linear fitting of mass specific I_F *versus* Pt mass loading (Fig. 3d), the highest mass peak current of Pt NPs in the hybrid films is estimated to be 362 mA mg^{-1}_{Pt}. Thus Pt-CVDG-3 achieves 70% of the maximum catalytic capacity of Pt NPs toward MOR, while those of most results reported in literatures are lower than about 200 mA mg^{-1}_{Pt} under similar conditions [28–32,42].

To further improve the MOR activity at lower potentials for practical DMFC applications, Ru was electrochemically deposited onto the Pt-CVDG films. With balanced coverage and dispersion, Pt-CVDG-2 was used for preparing PtRu-CVDG electrode. Fig. 4a shows the CV curves in 0.1 mol L^{-1} $HClO_4$ solution for Pt-CVDG-2 and Pt_xRu_y-CVDG electrodes (x and y represent the nominal coverage of Pt and Ru at the surface with $x+y=1$), which were prepared by depositing Ru for 20, 40, 60 and 80 potential cycles, respectively, in the potential range of −0.10–0.20 V and at a scan rate of 50 mV s^{-1}. To further evaluate the chemical composition of the PtRu-CVDG hybrids, XPS were carried out on PtRu-CVDG, as shown in Fig. S4c. The peak at about 462 eV (Ru 3p) illustrates the existence of Ru. The chemical state of Ru has been further confirmed by using the Ru 3p spectrum rather than Ru 3d because of the overlap between the Ru 3d and C 1s spectra. As shown in Fig. S4d, the Ru $3p_{3/2}$ spectrum could be fitted into three peaks located at 462.2, 464.3 and 466.3 eV, corresponding to metallic Ru, RuO_2 and RuO_xH_y, respectively. The formation of oxide states might result from the slight oxidation of Ru upon exposure to air. The MOR activity of Pt_xRu_y-CVDG films was measured by CV in a mixture solution containing 0.1 mol L^{-1} $HClO_4$ + 2.0 mol L^{-1} CH_3OH. From Fig. 4b, the mass specific current density of PtRu-CVDG film catalysts at 0.50 V are 222.5, 280.3, 223.75 and 122.4 mA mg^{-1}_{Pt} after deposition of Ru for 20, 40, 60 and 80 potential cycles, respectively, all higher than 111.9 mA mg^{-1}_{Pt}, of the pristine Pt-CVDG-2 at 0.50 V. The highest MOR current is obtained from PtRu-CVDG film with the nominal Ru coverage 32%, which was about 2.5 times higher than pristine Pt-CVDG-2 at 0.50 V. The onset potential of $Pt_{0.68}Ru_{0.32}$-CVDG for MOR shifts to 0.25 V, which is about 0.20 V more negative than that from Pt-CVDG-2 (0.45 V). The higher MOR activity of PtRu-CVDG films may be related to the highly dispersed capping-agent-free Pt NPs on CVDG and the good distribution of Ru on Pt NPs [63], and it is well accepted that the strong adsorption of hardly-oxidized CO on Pt surface leads to the self-poisoning [8]. The higher MOR activity for PtRu can be explained by two effects: 1) ensemble effect in which Ru adsorbs OH at the lower potential than Pt so that CO adsorbed on Pt can be oxidized to CO_2 more easily; 2) electric effect in which the

electron-charge transfer from Ru to Pt makes the Pt–CO bond weaker and more suitable to oxidize methanol [16]. In the electro-deposition of Ru on Pt NPs [17], the contact between Pt and Ru increases with the number of deposition cycles, leading to the increased catalytic activity till the Ru coverage of 32% (Fig. 4b). But the further deposition of Ru may cover more Pt active sites, thus deteriorates the MOR activity for higher Ru contents [12].

In summary, we have demonstrated the preparation of Pt NPs films supported by CVDG using a simple and cost-effective method. The obtained Pt-CVDG films have advantages of uniform dispersion of Pt NPs, transferability and structural stability. When being used as an anode of DMFCs, the hybrid films exhibit excellent electro-catalytic activity and high poison tolerance, which can be attributed to the high utilization of Pt atoms dispersed on CVDG and the excellent electric conductivity of the films. Meanwhile, the mass load of Pt (80–89 wt.%) in Pt-CVDG hybrids was greatly increased compared with that of traditional Pt-carbon hybrid catalyst (20 wt.%). In addition, the introduction of Ru has further improved the methanol oxidation activity. The optimized PtRu-CVDG film has a nominal Pt and Ru coverage ratio of 2:1, from which the onset potential is 0.24 V *vs*. Ag/AgCl and the mass activity of Pt is 2.5 times higher than that of Pt-CVDG film. In principle, the method can be applied to other metal NPs for fabrication of high-performance CVDG-based nanostructure. We believe that this synthesis strategy can be also extended to more applications such as sensors, electronic devices, information storage, biomedicine and more.

Received 22 August 2018; accepted 9 October 2018; published online 14 November 2018

1 Reddington E, Sapienza A, Gurau B, *et al.* Combinatorial electrochemistry: a highly parallel, optical screening method for discovery of better electrocatalysts. Science, 1998, 280: 1735–1737
2 Paik Y, Kim SS, Han OH. Methanol behavior in direct methanol fuel cells. Angew Chem Int Ed, 2008, 47: 94–96
3 Tiwari JN, Tiwari RN, Singh G, *et al.* Recent progress in the development of anode and cathode catalysts for direct methanol fuel cells. Nano Energy, 2013, 2: 553–578
4 Bahrami H, Faghri A. Review and advances of direct methanol fuel cells: Part II: Modeling and numerical simulation. J Power Sources, 2013, 230: 303–320
5 Tian XL, Wang L, Deng P, *et al.* Research advances in unsupported Pt-based catalysts for electrochemical methanol oxidation. J Energy Chem, 2017, 26: 1067–1076
6 Li M, Zhao Z, Cheng T, *et al.* Ultrafine jagged platinum nanowires enable ultrahigh mass activity for the oxygen reduction reaction. Science, 2016, 354: 1414–1419
7 Cao D, Lu GQ, Wieckowski A, *et al.* Mechanisms of methanol decomposition on platinum: a combined experimental and *ab initio* approach. J Phys Chem B, 2005, 109: 11622–11633
8 Chen YX, Miki A, Ye S, *et al.* Formate, an active intermediate for direct oxidation of methanol on Pt electrode. J Am Chem Soc, 2003, 125: 3680–3681
9 Xue Q, Xu G, Mao R, *et al.* Polyethyleneimine modified AuPd@PdAu alloy nanocrystals as advanced electrocatalysts towards the oxygen reduction reaction. J Energy Chem, 2017, 26: 1153–1159
10 Ma SY, Li HH, Hu BC, *et al.* Synthesis of low Pt-based quaternary PtPdRuTe nanotubes with optimized incorporation of Pd for enhanced electrocatalytic activity. J Am Chem Soc, 2017, 139: 5890–5895
11 Wei ZD, Li LL, Luo YH, *et al.* Electrooxidation of methanol on upd-Ru and upd-Sn modified Pt electrodes. J Phys Chem B, 2006, 110: 26055–26061
12 Yao Y, Cai J, Zheng Y, *et al.* Preparation of surfactant-free Pt and PtRu nanoparticles with high activity for methanol oxidation. Chin J Chem Phys, 2014, 27: 332–336
13 Fu QQ, Li HH, Ma SY, *et al.* A mixed-solvent route to unique PtAuCu ternary nanotubes templated from Cu nanowires as efficient dual electrocatalysts. Sci China Mater, 2016, 59: 112–121
14 Petrii OA. Pt–Ru electrocatalysts for fuel cells: a representative review. J Solid State Electrochem, 2008, 12: 609–642
15 Tao Q, Chen W, Yao Y, *et al.* Study on methanol oxidation at Pt and PtRu electrodes by combining *in situ* infrared spectroscopy and differential electrochemical mass spectrometry. Chin J Chem Phys, 2014, 27: 541–547
16 Chatterjee M, Chatterjee A, Ghosh S, *et al.* Electro-oxidation of ethanol and ethylene glycol on carbon-supported nano-Pt and -PtRu catalyst in acid solution. Electrochim Acta, 2009, 54: 7299–7304
17 Frelink T, Visscher W, van Veen JAR. Measurement of the Ru surface content of electrocodeposited PtRu electrodes with the electrochemical quartz crystal microbalance: implications for methanol and CO electrooxidation. Langmuir, 1996, 12: 3702–3708
18 Coutanceau C, Rakotondrainibé AF, Lima A, *et al.* Preparation of Pt–Ru bimetallic anodes by galvanostatic pulse electrodeposition: characterization and application to the direct methanol fuel cell. J Appl Electrochem, 2004, 34: 61–66
19 Huang H, Sun D, Wang X. Low-defect MWNT–Pt nanocomposite as a high performance electrocatalyst for direct methanol fuel cells. J Phys Chem C, 2011, 115: 19405–19412
20 Jiang H, Zhao T, Li C, *et al.* Functional mesoporous carbon nanotubes and their integration *in situ* with metal nanocrystals for enhanced electrochemical performances. Chem Commun, 2011, 47: 8590–8592
21 Zhang H, Ren W, Guan C, *et al.* Pt decorated 3D vertical graphene nanosheet arrays for efficient methanol oxidation and hydrogen evolution reactions. J Mater Chem A, 2017, 5: 22004–22011
22 Huang W, Wang H, Zhou J, *et al.* Highly active and durable methanol oxidation electrocatalyst based on the synergy of platinum–nickel hydroxide–graphene. Nat Commun, 2015, 6: 10035
23 Dong L, Gari RRS, Li Z, *et al.* Graphene-supported platinum and platinum–ruthenium nanoparticles with high electrocatalytic activity for methanol and ethanol oxidation. Carbon, 2010, 48: 781–787

24 Li Y, Gao W, Ci L, *et al.* Catalytic performance of Pt nanoparticles on reduced graphene oxide for methanol electro-oxidation. Carbon, 2010, 48: 1124–1130
25 Guo S, Dong S, Wang E. Three-dimensional Pt-on-Pd bimetallic nanodendrites supported on graphene nanosheet: facile synthesis and used as an advanced nanoelectrocatalyst for methanol oxidation. ACS Nano, 2010, 4: 547–555
26 Gotterbarm K, Späth F, Bauer U, *et al.* Reactivity of graphene-supported Pt nanocluster arrays. ACS Catal, 2015, 5: 2397–2403
27 Huang H, Yang S, Vajtai R, *et al.* Pt-decorated 3D architectures built from graphene and graphitic carbon nitride nanosheets as efficient methanol oxidation catalysts. Adv Mater, 2014, 26: 5160–5165
28 Bo X, Guo L. Simple synthesis of macroporous carbon–graphene composites and their use as a support for Pt electrocatalysts. Electrochim Acta, 2013, 90: 283–290
29 Choi SM, Seo MH, Kim HJ, *et al.* Synthesis of surface-functionalized graphene nanosheets with high Pt-loadings and their applications to methanol electrooxidation. Carbon, 2011, 49: 904–909
30 Huang H, Chen H, Sun D, *et al.* Graphene nanoplate-Pt composite as a high performance electrocatalyst for direct methanol fuel cells. J Power Sources, 2012, 204: 46–52
31 Li Y, Tang L, Li J. Preparation and electrochemical performance for methanol oxidation of Pt/graphene nanocomposites. Electrochem Commun, 2009, 11: 846–849
32 Zhang LS, Liang XQ, Song WG, *et al.* Identification of the nitrogen species on N-doped graphene layers and Pt/NG composite catalyst for direct methanol fuel cell. Phys Chem Chem Phys, 2010, 12: 12055
33 Bagri A, Mattevi C, Acik M, *et al.* Structural evolution during the reduction of chemically derived graphene oxide. Nat Chem, 2010, 2: 581–587
34 Pei S, Cheng HM. The reduction of graphene oxide. Carbon, 2012, 50: 3210–3228
35 Li N, Cao M, Hu C. Review on the latest design of graphene-based inorganic materials. Nanoscale, 2012, 4: 6205–6218
36 Yao Y, Chen W, Du Y, *et al.* An electrochemical *in situ* infrared spectroscopic study of graphene/electrolyte interface under attenuated total reflection configuration. J Phys Chem C, 2015, 119: 22452–22459
37 Chien CC, Jeng KT. Effective preparation of carbon nanotube-supported Pt–Ru electrocatalysts. Mater Chem Phys, 2006, 99: 80–87
38 Zamborini FP, Hicks JF, Murray RW. Quantized double layer charging of nanoparticle films assembled using carboxylate/(Cu^{2+} or Zn^{2+})/carboxylate bridges. J Am Chem Soc, 2000, 122: 4514–4515
39 Schmitt J, Decher G, Dressick WJ, *et al.* Metal nanoparticle/polymer superlattice films: fabrication and control of layer structure. Adv Mater, 1997, 9: 61–65
40 Sarathy KV, Thomas PJ, Kulkarni GU, *et al.* Superlattices of metal and metal−semiconductor quantum dots obtained by layer-by-layer deposition of nanoparticle arrays. J Phys Chem B, 1999, 103: 399–401
41 Song J, Kam FY, Png RQ, *et al.* A general method for transferring graphene onto soft surfaces. Nat Nanotech, 2013, 8: 356–362
42 Zhou YG, Chen JJ, Wang F, *et al.* A facile approach to the synthesis of highly electroactive Pt nanoparticles on graphene as an anode catalyst for direct methanol fuel cells. Chem Commun, 2010, 46: 5951–5953
43 Liang Q, Zhang L, Cai M, *et al.* Preparation and charaterization of Pt/functionalized graphene and its electrocatalysis for methanol oxidation. Electrochim Acta, 2013, 111: 275–283
44 Mayavan S, Jang HS, Lee MJ, *et al.* Enhancing the catalytic activity of Pt nanoparticles using poly sodium styrene sulfonate stabilized graphene supports for methanol oxidation. J Mater Chem A, 2013, 1: 3489–3494
45 Qiu JD, Wang GC, Liang RP, *et al.* Controllable deposition of platinum nanoparticles on graphene as an electrocatalyst for direct methanol fuel cells. J Phys Chem C, 2011, 115: 15639–15645
46 Wang L, Tian C, Wang H, *et al.* Mass production of graphene *via* an *in situ* self-generating template route and its promoted activity as electrocatalytic support for methanol electroxidization. J Phys Chem C, 2010, 114: 8727–8733
47 Rajesh , Paul RK, Mulchandani A. Platinum nanoflowers decorated three-dimensional graphene–carbon nanotubes hybrid with enhanced electrocatalytic activity. J Power Sources, 2013, 223: 23–29
48 Zhong JP, Fan YJ, Wang H, *et al.* Copper phthalocyanine functionalization of graphene nanosheets as support for platinum nanoparticles and their enhanced performance toward methanol oxidation. J Power Sources, 2013, 242: 208–215
49 Li X, Cai W, An J, *et al.* Large-area synthesis of high-quality and uniform graphene films on copper foils. Science, 2009, 324: 1312–1314
50 Mao H, Wang R, Zhong J, *et al.* Mildly O_2 plasma treated CVD graphene as a promising platform for molecular sensing. Carbon, 2014, 76: 212–219
51 Ferrari AC, Basko DM. Raman spectroscopy as a versatile tool for studying the properties of graphene. Nat Nanotech, 2013, 8: 235–246
52 Nourbakhsh A, Cantoro M, Vosch T, *et al.* Bandgap opening in oxygen plasma-treated graphene. Nanotechnology, 2010, 21: 435203
53 Xiao N, Dong X, Song L, *et al.* Enhanced thermopower of graphene films with oxygen plasma treatment. ACS Nano, 2011, 5: 2749–2755
54 Bragaru A, Vasile E, Obreja C, *et al.* Pt nanoparticles on graphene–polyelectrolyte nanocomposite: Investigation of H_2O_2 and methanol electrocatalysis. Mater Chem Phys, 2014, 146: 538–544
55 Zhao J, Li H, Liu Z, *et al.* An advanced electrocatalyst with exceptional eletrocatalytic activity *via* ultrafine Pt-based trimetallic nanoparticles on pristine graphene. Carbon, 2015, 87: 116–127
56 Rhee CK, Kim BJ, Ham C, *et al.* Size effect of Pt nanoparticle on catalytic activity in oxidation of methanol and formic acid: comparison to Pt(111), Pt(100), and polycrystalline Pt electrodes. Langmuir, 2009, 25: 7140–7147
57 Meyer JC, Geim AK, Katsnelson MI, *et al.* On the roughness of single- and bi-layer graphene membranes. Solid State Commun, 2007, 143: 101–109
58 Ghosh K, Kumar M, Wang H, *et al.* Facile decoration of platinum nanoparticles on carbon-nitride nanotubes *via* microwave-assisted chemical reduction and their optimization for field-emission application. J Phys Chem C, 2010, 114: 5107–5112
59 Xu X, Zhou Y, Lu J, *et al.* Single-step synthesis of PtRu/N-doped graphene for methanol electrocatalytic oxidation. Electrochim Acta, 2014, 120: 439–451
60 Clavilier J, Armand D. Electrochemical induction of changes in the distribution of the hydrogen adsorption states on Pt (100) and Pt (111) surfaces in contact with sulphuric acid solution. J Electroanal

Chem Interfacial Electrochem, 1986, 199: 187–200
61 Herrero E, Franaszczuk K, Wieckowski A. Electrochemistry of methanol at low index crystal planes of platinum: an integrated voltammetric and chronoamperometric study. J Phys Chem, 1994, 98: 5074–5083
62 Sharma S, Ganguly A, Papakonstantinou P, *et al.* Rapid microwave synthesis of CO tolerant reduced graphene oxide-supported platinum electrocatalysts for oxidation of methanol. J Phys Chem C, 2010, 114: 19459–19466
63 Tripković AV, Popović KD, Grgur BN, *et al.* Methanol electrooxidation on supported Pt and PtRu catalysts in acid and alkaline solutions. Electrochim Acta, 2002, 47: 3707–3714

Acknowledgements We acknowledge the support from the National Natural Science Foundation of China (51322204 and 51772282), the National Program on Key Basic Research Project (973 Program and 2015CB932300) and the Fundamental Research Funds for the Central Universities (WK2060140014 and WK2060140017).

Author contributions Tao Z designed and engineered the samples; Tao Z, Chen W and Yang J performed the experiments; Tao Z, Chen W, Yang J, Wang X, Tan Z and Ye J performed the data analysis; Tao Z wrote the paper with support from Zhu Y and Chen Y. All authors contributed to the general discussion.

Conflict of interest The authors declare no competing financial interest.

Supplementary information Experiment section and the supporting data are available in the online version of the paper.

Zhuchen Tao received his bachelor's degree in materials chemistry from the University of Science and Technology of China (USTC) in 2012. Then, he pursues his PhD degree in materials physics and chemistry under the supervision of Prof. Yanwu Zhu at USTC. His research interest focuses on the electrocatalytic performance of carbon-related films.

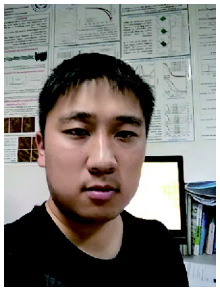

Wei Chen is currently a PhD candidate at USTC in the group of Prof. Chen. His research focuses on using *in-situ* spectroscopic methods such as differential electrochemical mass spectrometry and *in-situ* electrochemical infrared spectrometry to study reaction mechanisms and kinetics of fundamental electrochemical reactions such as hydrogen evolution/oxidation, oxygen reduction, and formic acid oxidation reactions.

Yan-Xia Chen is a professor at USTC. She gained her PhD degree under the supervision of Prof. Zhong Qun Tian at Xiamen University, China. Her research covers spectro-electrochemistry, single crystal electrochemistry, and electrocatalysis and focuses on developing spectroscopic methods with both qualitative and quantitative analytical functions and using them in fundamental studies on electrochemical interfacial structure, reaction mechanisms, and kinetics of fuel cell processes.

Yanwu Zhu received his PhD in 2007 from the Department of Physics, National University of Singapore. After years as postdoctoral researcher at National University of Singapore and The University of Texas at Austin, he joined USTC as a professor in 2011. His current research interest includes the preparation of novel carbon materials and their applications in energy storage and conversion.

超薄可转移的铂和铂钌修饰的石墨烯薄膜作为高效甲醇氧化催化剂

陶柱晨[1†], 陈微[2†], 杨晶[2], 王向阳[1], 谈紫琪[1], 叶江林[1], 陈艳霞[2*], 朱彦武[1*]

摘要 从氧化石墨中获得石墨烯材料在负载金属催化剂中具有很大的应用潜力，但在通过化学气相沉积制备的高质量石墨烯(CVDG)上均匀负载金属纳米粒子仍然是一个挑战. 我们成功制备了在CVDG上均匀负载具有约3.3 nm尺寸的铂纳米粒子的超薄复合薄膜(Pt-CVDG)，并且这种薄膜可通过类似CVDG转移的方法转移到目标衬底上. Pt-CVDG薄膜在甲醇催化氧化中表现出优异的性能，具有高达94.1 $m^2\ g^{-1}_{Pt}$的电化学活性表面积，并且在0.7 V下具有293.1 mA mg^{-1}_{Pt}的高质量活性电流密度，该电流密度几乎是相同条件下商业Pt/C的两倍. 此外，为进一步提高催化性能，将钌沉积到Pt-CVDG薄膜上，在Ru覆盖率达到50%时得到比原始样品高2倍的催化电流密度且催化起始电位降低0.2 V. 同时这种基于CVDG的复合薄膜为评估Pt NPs-碳杂化催化剂性能的极限提供了一个简单模型.

